

Experimental and theoretical study of demagnetization fields in superconducting samples of orthorhombic shape

C. Navau

Grupo d'Electromagnetisme (Department de Física), Universitat Autònoma de Barcelona, 08192 Bellaterra, Barcelona, Catalonia, Spain and Escola Universitària Salesiana de Sarrià, Sant Joan Bosco 74, 08017 Barcelona, Catalonia, Spain

C. A. Cardoso

Grupo de Materiais e Dispositivos (Departamento de Física), Centro Multidisciplinar de Desenvolvimento de Materiais Cerâmicos (CMDMC), Universidade Federal de São Carlos, Caixa Postal 676, São Carlos SP, 13565-905, Brazil

O. F. de Lima

Instituto de Física, Gleb Wataghin, Universidade Estadual de Campinas, Campinas SP, 13083-970, Brazil

F. M. Araujo-Moreira^{a)}

Grupo de Materiais e Dispositivos (Departamento de Física), Centro Multidisciplinar de Desenvolvimento de Materiais Cerâmicos (CMDMC), Universidade Federal de São Carlos, Caixa Postal 676, São Carlos SP, 13565-905, Brazil

(Received 23 June 2003; accepted 10 March 2004)

In this work we present a model for the calculation of the magnetic properties of superconductors of orthorhombic shape in the perfect shielding state when an external uniform magnetic field is applied in the direction of one of the principal axes of the sample. Our model accounts for demagnetization effects and it is free of fitting parameters and boundary value conditions. We consider planar linear circuits that lie perpendicular to the direction of the applied field. Calculation of the value of the currents is based on magnetic energy minimization. The model is proved to be accurate enough to reproduce experimental results as long as the dimension along the applied field is not much lower than the other dimensions. Calculations of surface currents, as well as measurements and calculations of magnetization and initial susceptibility, are reported. We also present an empirical formula that provides a good fit to the initial susceptibility of a general sample of orthorhombic shape. Demagnetization effects observed on the experimental results are explained in terms of the induced currents in the superconductor. © 2004 American Institute of Physics. [DOI: 10.1063/1.1736325]

I. INTRODUCTION

When a superconducting or magnetic sample is in the presence of an applied magnetic field, it becomes magnetized. Therefore, magnetic poles appear over some regions of the material, and produce a magnetic field that depends on the geometry of the sample. Thus, measurements of the magnetic properties could be strongly dependent on the shape of the sample under study.

When a magnetic field is applied to the sample, the total field can be considered the sum of the applied field, \mathbf{H}_a , and the field created by the currents induced \mathbf{H}_J :

$$\mathbf{H} = \mathbf{H}_a + \mathbf{H}_J. \quad (1)$$

The induced currents result in magnetization of the superconductor, \mathbf{M} , and in the demagnetization field \mathbf{H}_d .

Besides some simple ideal cases where one or more dimensions are infinite, only in ellipsoidal-shaped samples with uniform applied field are the demagnetization field and the magnetization uniform. In this particular situation, geo-

metric demagnetizing effects can be summarized by a scalar factor, N , which depends on the dimensions of the ellipsoid.¹

For other finite geometries, the study of demagnetizing fields is a complicated task, mainly because the demagnetizing field is nonuniform inside the sample. In this case, the Maxwell equations should be solved numerically. In the case of finite cylinders with applied field along the principal axis, an important contribution was made by Chen *et al.*² These authors described a numerical procedure to obtain both fluxmetric and magnetometric demagnetizing factors for different magnetic susceptibility of the cylinders. In the case of prisms, results for demagnetization factors are reported for zero susceptibility^{3,4} and infinite susceptibility in the case of square bars.⁵ Recently, a study was reported for an infinite bar with a square cross section, and it included analytical expressions for extreme values of susceptibility⁶ and numerical expressions for intermediate values.⁷ All of that work included results for current distribution and magnetization and demagnetization factors (both fluxmetric and magnetometric).

Superconductors can be considered a particular case of magnetic materials. Below the lower critical magnetic field both type-I and type-II superconductors behave as perfect

^{a)}Corresponding author; electronic mail: faraujo@df.ufscar.br

diamagnets, excluding the external magnetic field from its interior. Thus, $\mathbf{H}=0$ inside such a superconductor, except over the magnetic penetration depth. In this situation, the total magnetic field inside the superconducting sample can be considered a result of the superposition of the external magnetic field and the field created by the induced superficial currents. Those currents are responsible for magnetization of the sample and for the existence of the demagnetizing field. Therefore, calculation of induced superficial currents will allow determination of the effect of the geometry of the sample in measured magnetic properties.

The Meissner state of a sample can also be viewed as the limiting case of high critical current of a type-II superconductor. In the more general case of a type-II superconductor, the current distribution that shields a thin superconductor of arbitrary shape (with the field applied perpendicular to its plane) was numerically solved by Prigozhin *et al.*⁸ using the critical state model.⁹ Penetration of current in finite type-II superconducting cylinders has also been studied.^{10–13} In a similar way, complete shielding is also a particular case (internal susceptibility equal to -1) in the general treatment of cylinders done in Ref. 2. Moreover, the case of a superconducting cylinder in the Meissner state, focusing especially on demagnetizing problems, has been shown in Ref. 14 from both the theoretical and the experimental point of view. In Refs. 15 and 16 shielding of a finite type-II cylindrical superconductor was studied in the case of a nonuniform (cylindrical symmetry) applied field. Of particular interest for the present work is the model described in Ref. 14 to calculate shielding currents: for finite cylinders, the model assumes a system of circular linear currents flowing through the surface of the superconductor. Minimization of the magnetic energy is, then, used to establish the value of the induced current at each circuit in order to completely shield the total magnetic field from inside the superconductor. It is important to note that the directions of induced currents have to be implemented *a priori*. In the case of cylinders, those directions are completely determined by the symmetry of the system.

In the case of samples of orthorhombic shape, symmetry arguments are not enough to completely determine the direction of induced currents. In particular, squared currents were considered in Ref. 17 to consider the fully penetrated critical state. In Ref. 18 squared currents that flow over the surface were considered in order to explain susceptibility measurements of niobium orthorhombically shaped samples with a square base in a completely shielded state. However, no systematic study of demagnetization effects was done.

In this article we apply the procedure of minimization of energy to simulate the Meissner state in a general three-dimensional sample of orthorhombic shape. In this case, the applied magnetic field was chosen to be along one of its principal axes. Rectangular induced currents were considered to flow on the surfaces of the superconductor. These currents represent an approximation of real currents which completely shield the applied magnetic field. The model presented here is not exact since the rectangular circuits do not completely shield the applied magnetic field. However, our model could be very useful for experimentalists, since it allows one to obtain accurate enough information about shield-

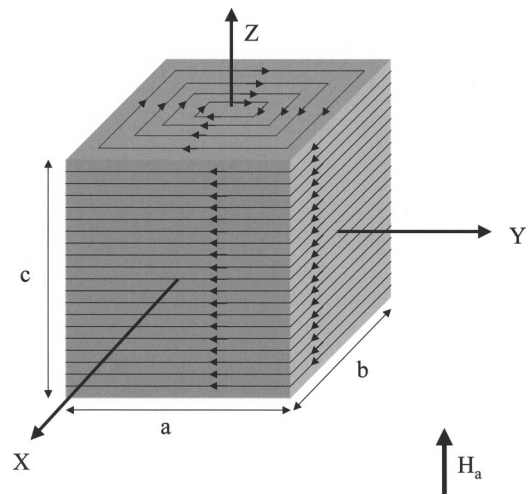


FIG. 1. Sketch of the geometry of the superconducting sample and assumed induced current circuits. The direction of the applied magnetic field is also shown.

ing of the superconducting sample. Besides, this model can be adapted to geometries other than the orthorhombic one, and it can be easily implemented in a personal computer.

This article is structured as follows. In Sec. II we review the calculation procedure and the conditions that the model should obey in order to be applicable. In Sec. III we show experimental and numerical results for magnetization and susceptibility as well as the calculated current distribution. In Sec. IV we discuss earlier results and the applicability of our model. Finally, conclusions are presented in Sec. V.

II. THEORETICAL MODEL

We consider a perfectly shielded superconducting sample of orthorhombic shape of dimensions a , b , and c . We consider also a uniformly applied magnetic field $\mathbf{H}_a = H_a \mathbf{k}$, oriented along the z axis, which is the direction of the c dimension of the superconducting sample. We assume $\lambda = 0$, where λ is the penetration depth of the magnetic field in the superconductor. We use rectangular coordinates that originate at the geometrical center of the superconducting sample (see Fig. 1).

Our aim is to calculate currents induced on the surface of the superconductor that shield the applied magnetic field. Using arguments of symmetry we can deduce some of the properties about the direction of the flowing induced currents. In the present case, currents must be symmetric with respect to the center layer of the superconductor (plane $z = 0$). They must also be antisymmetric (because of the sign) with respect to the z axis. That is,

$$\begin{aligned} \mathbf{K}(x, y, -z) &= \mathbf{K}(x, y, z), \\ \mathbf{K}(-x, -y, z) &= -\mathbf{K}(x, y, z). \end{aligned} \tag{2}$$

In these equations $\mathbf{K}(x, y, z)$ is the surface current density at the point (x, y, z) belonging to the surface of the superconductor. It is clear that the current density induced $\mathbf{K}(x, y, 0)$ must close itself in a rectangular circuit lying on the $z = 0$ plane and follow the rectangular shape of the surface of the superconductor.

To accomplish these symmetry arguments we can consider rectangular currents flowing in planes perpendicular to the applied magnetic field. This choice is not the only option in order to accomplish symmetry conditions [Eqs. (2)]. In fact, for the case of $c \ll a$ the model is expected to fail since the induced currents are known to be nonrectangular in the center region of the surfaces, $z = \pm c/2$.^{8,11}

For simplicity, instead of considering surface currents, we substitute them by a set of linear currents that flow through the surface of the superconductor (Fig. 1). Once the direction of the induced currents is set in advance, we calculate their values by the energy minimization method presented in Ref. 14. The method of calculation consists of increasing step by step the value of the current in some of the circuits considered after turning on applied magnetic field H_a . The circuit chosen would be the one where the increment of the absolute value of its current will give maximum energy minimization of the whole system. This method is equivalent to considering a set of N rectangular circuits distributed over the sample's surface, and consider that, in the presence of applied field, the currents in the individual circuits I_i , ($i=1,2,\dots,N$), are chosen such that the magnetic flux Φ_i through every circuit is zero. This equivalence can be shown from the following formulation.

Consider $N+1$ circuits, with $i=0$ corresponding to a loop of radius R (much larger than dimensions a , b , and c) carrying current I_0 and generating applied field $H_a = I_0/2R$ at the center of the loop where we place the superconducting samples (considered a set of N screening rectangular circuits). The total magnetic energy can be written as

$$E = \frac{1}{2} L_0 I_0^2 + \sum_{i=1}^N M_{0i} I_0 I_i + \frac{1}{2} \sum_{i=1}^N L_i I_i^2 + \frac{1}{2} \sum_{i=1}^N \sum_{j=1, j \neq i}^N M_{ij} I_i I_j, \quad (3)$$

where M_{ij} is the mutual inductance between circuits i and j . The terms,

$$M_{0i} I_0 = \frac{\mu_0 a_i b_i}{2R} I_0 = \Phi_{0i}, \quad (4)$$

are the contribution of the applied magnetic field to the magnetic flux through circuit i . The variation of energy upon changing the current values in the sample is

$$\delta E = \sum_{i=1}^N \left(\Phi_{0i} + L_i I_i + \sum_{j=1, j \neq i}^N M_{ij} I_j \right) \delta I_i. \quad (5)$$

Since this holds for any δI_i , we conclude

$$\Phi_{0i} + L_i I_i + \sum_{j=1, j \neq i}^N M_{ij} I_j = 0. \quad (6)$$

The left side of Eq. (6) is the total flux through circuit i , Φ_i . So, we have demonstrated that consideration of the energy minimization leads to $\Phi_i = 0$ for all i . From Eq. (6) and defining $M_{ii} = L_i$, we note that one could obtain the value of the currents induced from the following expression:

$$I_j = - \sum_{i=1}^N M_{ij}^{-1} \Phi_{0i}. \quad (7)$$

The expressions for mutual inductance between rectangular circuits with the geometrical center in the same axis (considered in this work) are reviewed in Appendix A.

Once currents I_i have been calculated, we can calculate the magnetization, which has only the z component, from

$$M_z = \frac{1}{V} \sum_i I_i a_i b_i, \quad (8)$$

where $V = abc$ is the volume of the superconducting sample. The real component of complex ac susceptibility can be calculated as the initial slope of the magnetization versus the applied magnetic field curve:

$$\chi' = \lim_{H_a \rightarrow 0} \frac{M_z}{H_a}. \quad (9)$$

In order to check the accuracy of our model we calculate the total magnetic field (created by currents superimposed on the applied field) inside the superconductor. The magnetic field is directly calculated from Biot-Savart law, adding the contribution of all linear rectangular currents (see Appendix B for the formulas).

We note that the model is just an approximation since rectangular currents over the surface of an orthorhombic sample do not exactly shield a uniformly applied magnetic field throughout its interior. However, the model presented, although approximate, is simple and accurate enough as long as $c \ll a$ is not considered. When applied to experimental data, the model is free of fitting parameters, and only the geometric dimensions of the sample should be implemented in the calculations.

III. RESULTS

A. Calculated surface current distribution

We have used the energy minimization procedure¹⁴ to calculate the induced current distribution of three different samples with different c dimensions along the direction of the applied field (see Fig. 2). In all the cases, we have considered $b = a$.

Figure 2 shows that the induced current on faces which are perpendicular to the applied magnetic field hardly depends on the dimension along it, c . This observation is also true in the case of infinitely long bars ($b \gg a$),⁶ and for finite cylinders.¹⁴ This means that, given an applied magnetic field, the induced currents that circulate on the top and the bottom faces of the superconductor create almost the same magnetic field, irrespective of the length of the sample. We observe that, close to the center of the top and bottom faces, the current increases linearly. When it reaches the edge of the orthorhomb, it diverges (actually, the divergence is a consequence of the discretization used and the consideration of $\lambda = 0$). On the lateral faces, a plateau of nearly constant current value is observed. As expected, the plateau is more extensive for longer samples and the value of the induced current density depends on the aspect ratio c/a . The value of the

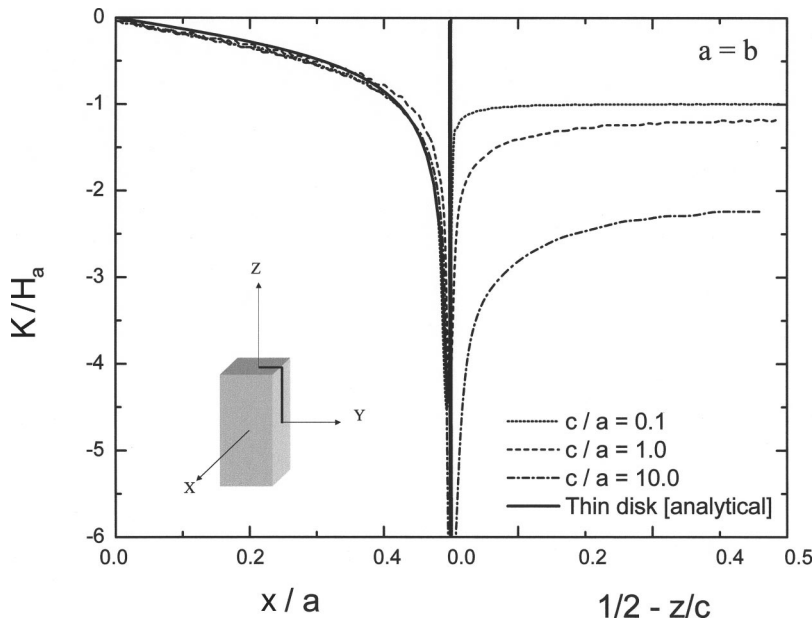


FIG. 2. Calculated surface induced current density for a square based ($b=a$) sample. Left: Current density on the bottom face of the superconductor along line $x \in (0, a/2)$, $y=0$, $z=c/2$. Right: Current density on the lateral face of the superconductor along line $x = a/2$, $y=0$, $z \in (c/2, 0)$. For comparison, we have also plotted (solid curve) the value of the current density on one face of a circular thin film disk or radius $R=a$ (after Ref. 19).

current at the plateau tends to be equal to the magnetic field applied when the value of c/a increases. In the trivial limit of a long square bar with uniformly applied magnetic field along the sample, $c \gg a$, the value of the induced superficial current density equals $-H_a$, exactly.

From the above behavior we observe that demagnetization fields come both from the faces perpendicular to the applied field and from the lateral faces. However, the top and bottom faces create a field that is very weakly dependent on ratio c/a , so its contribution to the demagnetization is quite independent of the value of c/a . Thus, the differences observed in the measurements of magnetic properties will arise chiefly from the different behavior of lateral faces, not only because of variation in the size of their extension but also because the currents induced there change as c/a does.

We also see in Fig. 2 that the induced current distribution on the top and bottom faces of a square-based sample of orthorhombic shape is not very different from that of a circular thin cylinder with radius equal to the semiside of the orthorhomb. For comparison, this last expression (known analytically¹⁹) is also plotted (solid line) in Fig. 2.

B. Experimental and calculated magnetization

We have measured the magnetization of two sets of high-quality niobium samples of orthorhombic shape (group Q: square base; group R: rectangular base). Their dimensions are summarized in Table I.

All samples were obtained from the same piece of niobium obtained after two electron-beam fusion processes. After machining, they were cleaned in an ultrasound bath, and later using a solution of HCl-HNO₃.

We have determined the crystallographic quality of all samples by both x-ray diffraction (XRD) and scanning electron microscopy (SEM). For XRD we used a Siemens D/5000 diffractometer and for SEM we used a JEOL JSM-5800/LV microscope.

Magnetic characterization was performed through both the magnetization as a function of the external dc magnetic field, $M(H_a)$, and the complex ac magnetic susceptibility as a function of the absolute temperature, $\chi(T)$. We performed the experiments using a Quantum Design MPMS5 superconducting quantum interference device (SQUID) magnetometer capable of operating in ranges of $2 \text{ K} < T < 400 \text{ K}$, $0.1 \text{ A/m} < h < 300 \text{ A/m}$, and $1 < f < 1000 \text{ Hz}$, where T , h and f are the absolute temperature, the amplitude, and the frequency of the ac magnetic field, respectively. In all cases, to avoid trapped magnetic flux, samples were zero field cooled (ZFC) before each experiment. The magnetic field was always applied along one axis of the sample.

In Fig. 3 we present our experimental results for magnetization of different samples, together with the magnetization calculated from Eq. (8) (shown by solid lines). We observe good agreement in the initial straight part of magnetization for the rectangular samples, and also for the squared samples, except for the thinner (lower c) samples. We observe that the model describes well the initial linear part of

TABLE I. Name and dimensions of the niobium samples measured. Note that for rectangular samples (R) the relation b/a is approximately 1.4 in all samples. The variation between nominal and real values of the dimensions is smaller than 2%.

Name	a (mm)	b (mm)	c (mm)
R1	1.44	2.04	6.52
R3	1.48	2.06	4.12
R5	1.44	2.06	2.04
R7	1.46	2.04	1.06
R9	1.44	2.06	0.32
Q1		1.48	0.36
Q3		1.42	1.02
Q5		1.46	1.98
Q7		1.44	4.05
Q9		1.50	6.50

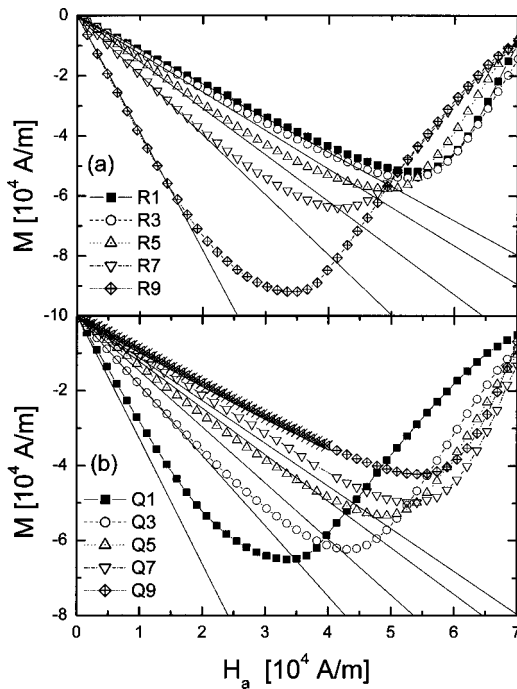


FIG. 3. Measured (symbols) and calculated (solid curves) initial magnetization of samples in Table I. (a) Samples with a rectangular base of ratio $b/a \approx 1.4$ and (b) samples with a square base.

the magnetization of a superconductor that corresponds to the range of fields in which it is in the completely shielded state, except for samples with $c \ll a$, as already stated. We also note that calculation of rectangular samples gives a better approximation than that for squared ones. We discuss this in Sec. IV. We observe that, for a fixed b/a ratio, the initial slope increases as the c/a ratio decreases because of increasing demagnetizing effects.¹⁴

C. Experimental, calculated, and approximate susceptibility

From the experimental magnetization results (Fig. 3), we can obtain values of the dc susceptibility. We also carried out measurements of the complex ac magnetic susceptibility for the two sets of samples. The results, together with the model calculations, after Eq. (9), are shown in Fig. 4.

In Fig. 4 we observe good agreement between experimental results and theoretical predictions, showing that our model is accurate enough to describe the susceptibility in samples of orthorhombic shape. As seen in Fig. 4, for fixed b/a , the susceptibility increases (in absolute value) as the sample gets thinner, and it tends toward -1 for very long samples, as expected. By fixing the c/a ratio, it is observed that the susceptibility is larger for rectangular samples (group R) than for square ones (group Q).

In Fig. 5 we show the theoretically calculated susceptibility for different b/a and c/a ratios. We can observe two different aspects. First, for a fixed b/a value, as dimension c decreases, the magnetic susceptibility increases (in absolute value) since demagnetization fields are more important at small c . In fact, for $c \ll a$, the fields due to the $z = \pm c/2$ planes give the most important contribution to the total field

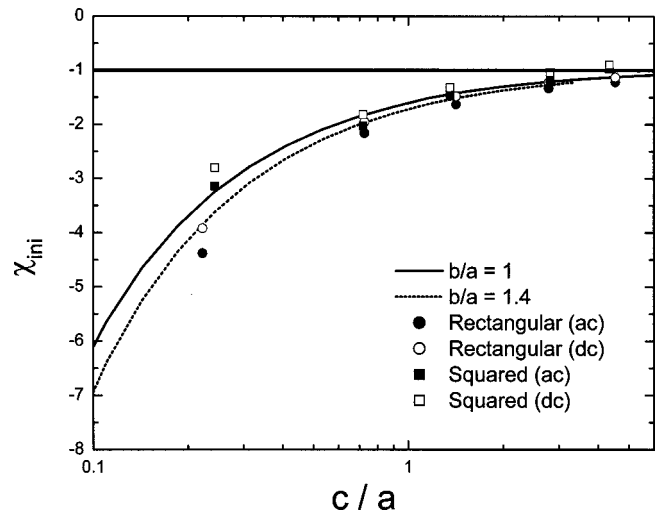


FIG. 4. Measured and calculated initial susceptibility for different samples in Table I. Open symbols correspond to ac magnetic susceptibility measurements; closed symbols correspond to the dc measurements. Curves show model calculations.

and magnetization (similar to the behavior found for cylinders¹⁴). For long c , the susceptibility tends toward -1 , indicating no demagnetization fields (the long sample oriented in the direction of applied magnetic field). On the other hand, by fixing the value of the c/a ratio and increasing b/a , the susceptibility increases in absolute value, reaching a maximum saturation value for a very large b/a ratio (i.e., a long bar with applied magnetic field transverse to the longer dimension). This limit has already been calculated.^{6,7} Moreover, when b/a becomes small, the susceptibility, as long as $c \approx a$, also tends toward -1 , since this case corresponds to a slab with a longitudinally applied magnetic field.

The values for the susceptibility can be readily approximated by a phenomenological expression which includes all the cases. Similar to the equation presented by Brandt¹¹ for

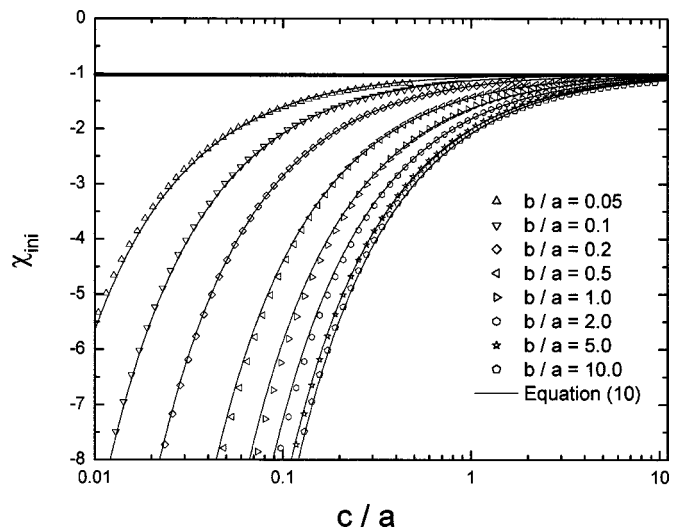


FIG. 5. Calculations of the initial susceptibility as a function of c/a for different values of the ratio b/a . Numerically calculated values are plotted by symbols, and values from the empirical formula [Eq. (10)] are shown by solid curves.

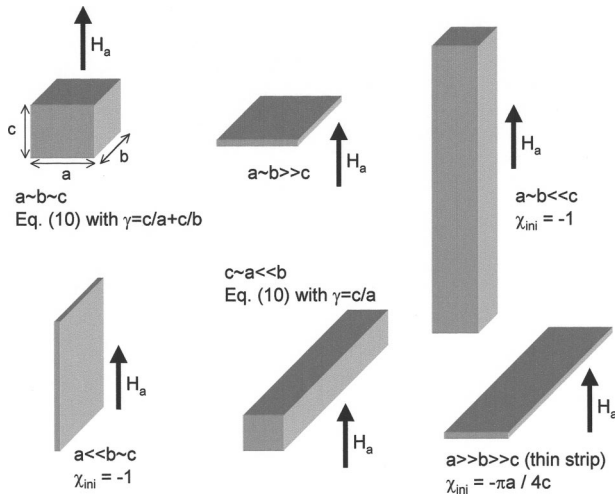


FIG. 6. Some geometries and their values of initial susceptibility calculated from the empirical formula, Eq. (10).

the case of finite cylinders, we can fit the calculated susceptibility results with a simple empirical formula:

$$\chi'_{ini} = -1 - \frac{\pi}{4\gamma} - \frac{\pi}{4\gamma} \tanh\left[\frac{\gamma}{2} \log\left(1 + \frac{2}{\gamma}\right)\right], \quad (10)$$

where the parameter γ is defined as

$$\gamma = \frac{c}{a} + \frac{c}{b}. \quad (11)$$

In Fig. 5 we have also plotted Eq. (10) for different values of b/a and c/a and compare them with the calculated values following the model presented.

We observe that Eq. (10) depends only on one parameter that includes all the geometrical dimensions of the system. In particular, for a thin strip, $b \gg a \gg c$, so $\gamma \rightarrow c/a \ll 1$. In this case Eq. (10) tends toward $-(\pi a / 4c)$ which agrees with the initial susceptibility for a thin strip calculated in Ref. 20. There are other interesting cases. For a long bar transverse to the applied field with a squared section ($c = a \ll b$) we obtain $\chi'_{ini} = -1 - 3\pi/8 = -2.178\,097$. For a cube ($a = b = c$), $\chi'_{ini} = -1 - \pi/5 = -1.628\,319$. In Fig. 6 we have plotted some interesting geometries and their initial susceptibility.

IV. DISCUSSION

Due to the symmetry of the system studied, the a and b dimensions are interchangeable. Moreover, the whole system can be scaled to either dimension a or b . Therefore, it is sufficient to calculate just those cases where $b > a$. For example, if we consider a the minimum dimension perpendicular to the direction of applied magnetic field, previous arguments have given

$$\begin{aligned} M_z(a,b,c) &= M_z(b,a,c) \\ &= M_z(1,b/a,c/a) = M_z(1,a/b,c/b), \end{aligned} \quad (12)$$

$$\begin{aligned} \chi'(a,b,c) &= \chi'(b,a,c) \\ &= \chi'(1,b/a,c/a) = \chi'(1,a/b,c/b). \end{aligned} \quad (13)$$

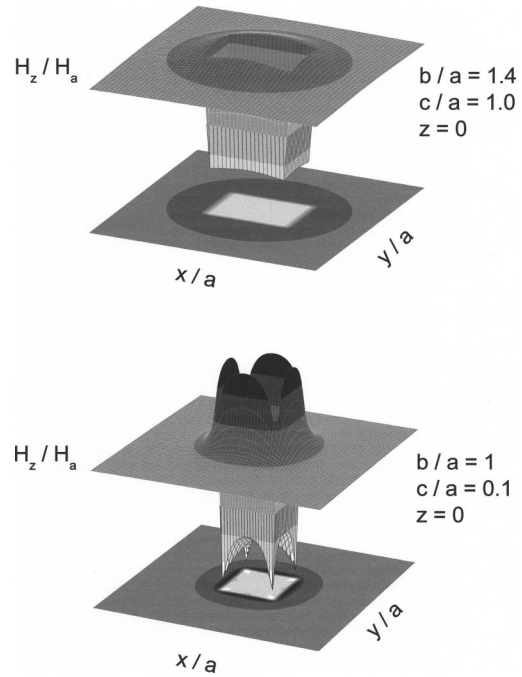


FIG. 7. Total magnetic field in the $z=0$ center plane. (Top) $b/a=1.4$, $c/a=1$; (bottom) $b/a=1$, $c/a=0.1$.

Therefore, these conditions allow calculation of the case of $b < a$ by calculating just its conjugated case. Since our model is more accurate for samples with a larger b/a ratio, it is straightforward to conclude that the least amount of accuracy is obtained for square-based samples $b = a$. Actually, as Eq. (10) shows, for a description of the susceptibility, the orthorhombic system can be described by only one parameter, $\gamma = c/a + c/b$.

As we have mentioned, as a consequence of our approximation of considering rectangularly shaped currents, the magnetic field applied is not fully shielded inside the superconductor. This is true even when the values of the flowing current minimize the magnetic energy. After the induced currents are determined, we can calculate the total field in any region of space just by adding the contribution of each current to the applied magnetic field. Even in the case of $b = a$, which is the ratio where the model is expected to be less accurate, the results obtained are good enough as long as c has a value not much lower than that of a . We show in Fig. 7 (bottom) the calculated z component of the magnetic field in the $z=0$ plane for a squared sample with $b = a$ and $c/a = 0.1$. Shielding of the applied magnetic field is not complete. This is directly related to the square shape of the model circuits. It is clear that this effect should decrease as c/a increases, or, alternatively, as b/a differs from unity. For comparison, we also show in Fig. 7 (top) the case for $b/a = 1.4$ and $c/a = 1$ which corresponds to one of the samples of group R. In this case, we observe that the shielding is much better, as expected.

There are several forms by which to quantify the accuracy of modeled circuits. For example, the magnitude $E = (V_{SC} B_a^2)^{-1} \int_{V_{SC}} |\mathbf{B}|^2 dV$, where V_{SC} is the volume of the superconductor and \mathbf{B} represents the total magnetic field calculated, gives an idea of the relative deviation of the calcu-

lated magnetic field from the complete shielding value (in exact shielding the above quantity should give a zero value). For the two cases shown in Fig. 7 we have obtained $E = 0.002$ for the rectangular $b/a = 1.4$, $c/a = 1.0$ case and $E = 0.022$ for the case of the $b/a = 1$, $c/a = 0.1$ sample. These quantities indicates that the shielding, even in the less accurate case, is good enough for most purposes, especially when we try to reproduce experimental data. We should note, however, that consideration of linear circuits makes the calculated field diverge very close to those circuits. In the previous calculations we have used 60×60 (face \times lateral) linear circuits for the rectangular sample and 130×30 circuits for the squared sample and we have evaluated the integral over the volume $x \in (-a/2 + a/100, a/2 - a/100)$, $y \in (-b/2 + b/100, b/2 - b/100)$, and $z \in (-c/2 + c/100, c/2 - c/100)$. We have found that our results are essentially unchanged when finer meshes are used.

V. CONCLUSIONS

In this work we have presented a numerical procedure which allows one to describe the measured magnetic properties of a superconductor in the completely shielded state. Our model is very simple, however very useful, since there are no fitting parameters and there is no need to impose boundary conditions. Although the induced current distribution obtained from the model is only approximate, it allows one to determine in an approximate way the picture of flowing induced currents that shield the magnetic field applied to samples of orthorhombic shape. Thus, it can be used to describe the demagnetization effects for them. In particular, calculation of the magnetization involves the integral of the currents. This means that details of the induced currents become blurred in calculation of the magnetization. Since the geometry we consider for the induced current distribution is not much different from the real one, the resulting calculated magnetization will have sufficient accuracy for practical use. Also, our model is appropriate for application to geometries other than orthorhombic whenever an approximate current distribution can be implemented. Actually, the calculation procedure for obtaining the current distribution gives exact results, within numerical accuracy, if the direction of the current induced can be established by symmetry arguments. This is particularly true for cylinders,¹⁴ even thin films, long bars with longitudinally applied field (the trivial case of shielding current with $K = H_a$), and long bars with transversely applied field (the limiting case of the model presented for $b \rightarrow \infty$ or $a \rightarrow \infty$).^{6,7}

Thus, using rectangular currents to model superconductors of orthorhombic shape, we have found that the induced current distribution over the faces perpendicular to the applied magnetic field is barely dependent on the length of the sample. The main differences in magnetic measurements between samples with different c/a ratios come from the different induced current distributions on the lateral faces. In this case, the field created by the perpendicular faces increases the value of the total field on the lateral faces over those regions close to the edges of the sample. This results in a larger value of current on those faces. For the lateral surface at points far from the edges, as the sample gets larger there is a plateau in the value of the surface current that (in magnitude) goes to H_a (which is the minimum value). Therefore, for thinner samples there is a larger average value of current induced, and it produces larger demagnetization effects. This is observed as larger initial slopes in the magnetization versus applied field curves, and corresponds to larger magnetic susceptibility.

ACKNOWLEDGMENTS

The authors gratefully acknowledge A. Sanchez and E. Pardo for stimulating discussions. This work was supported by MCyT (Project No. BFM2000-0001), CIRIT (Project No. 1999SGR00340), and CNPq and FAPESP (Brazil agencies). One of the authors (C.N.) acknowledges financial support from FAPESP (Grant No. 02/05319-0) and the hospitality of the Departamento de Física of Universidade Federal de São Carlos.

APPENDIX A: MUTUAL INDUCTANCE BETWEEN RECTANGULAR CENTERED LINEAR CIRCUITS

A key issue for using the model presented here is its simplicity and its easily reproducible procedure. However, the mutual inductance values that enter into the calculation are not straightforward. In any case, we can find its analytical expression by using the Neumann formula.²¹ To do this, we consider two rectangular circuits lying on parallel planes separated by a distance h , centered between their geometrical centers, with their sides parallel in pairs. Consider the first circuit with dimensions of b and a , and the second one with d and c along the x and y axes, respectively.

We define $F(t_1, t_2, t_3)$ as

$$\begin{aligned}
 F(t_1, t_2, t_3) = & \int_{t_1}^{-t_1} dx_1 \int_{t_2}^{-t_2} dx_2 \frac{1}{\sqrt{t_3^2 + (x_1 - x_2)^2}} = \sqrt{(t_1 - t_2)^2 + t_3^2} - \sqrt{(-t_1 - t_2)^2 + t_3^2} - \sqrt{(t_1 + t_2)^2 + t_3^2} + \sqrt{(-t_1 + t_2)^2 + t_3^2} \\
 & + t_2 \log[-t_1 + t_2 + \sqrt{(t_1 - t_2)^2 + t_3^2}] + t_1 \log[t_1 - t_2 + \sqrt{(t_1 - t_2)^2 + t_3^2}] - t_2 \log[-t_1 - t_2 + \sqrt{(-t_1 - t_2)^2 + t_3^2}] \\
 & - t_1 \log[t_1 + t_2 + \sqrt{(-t_1 - t_2)^2 + t_3^2}] - t_2 \log[t_1 + t_2 + \sqrt{(t_1 + t_2)^2 + t_3^2}] - t_1 \log[-t_1 - t_2 + \sqrt{(t_1 + t_2)^2 + t_3^2}] \\
 & + t_2 \log[-t_1 + t_2 + \sqrt{(-t_1 + t_2)^2 + t_3^2}] + t_1 \log[t_1 - t_2 + \sqrt{(-t_1 + t_2)^2 + t_3^2}].
 \end{aligned} \tag{A1}$$

The mutual inductance between two rectangular coils is

$$M = \frac{2\mu_0}{4\pi} (F\{a/2, c/2, \sqrt{[(b-d)/2]^2 + h^2}\} + F\{a/2, -c/2, \sqrt{[(b+d)/2]^2 + h^2}\} + F\{-b/2, -d/2, \sqrt{[(a-c)/2]^2 + h^2}\} + F\{-b/2, d/2, \sqrt{[(a+c)/2]^2 + h^2}\}). \quad (A3)$$

APPENDIX B: MAGNETIC FIELD DUE TO A RECTANGULARLY SHAPED CIRCUIT

Consider a planar (in the xy plane), rectangularly shaped circuit of dimensions b and a along the x and y axes, respectively. Consider that the circuit carries current I . The origin is taken to be the geometrical center of the circuit.

We can calculate the vector potential created by the linear current. We define

$$G(t_1, t_2, t_3, t_4) = \ln \left[\frac{t_2 - t_4 + \sqrt{(t_2 - t_4)^2 + t_3^2}}{t_1 - t_4 + \sqrt{(t_1 - t_4)^2 + t_3^2}} \right]. \quad (B1)$$

Vector potential \mathbf{A} at $\mathbf{r} = x\mathbf{i} + y\mathbf{j} + z\mathbf{k}$ has two components:

$$A_x = IG[-b/2, b/2, \sqrt{(y-a/2)^2 + z^2}, x] + IG[b/2, -b/2, \sqrt{(y+a/2)^2 + z^2}, x], \quad (B2)$$

$$A_y = IG[a/2, -a/2, \sqrt{(x-b/2)^2 + z^2}, y] + IG[-a/2, a/2, \sqrt{(x+b/2)^2 + z^2}, y]. \quad (B3)$$

We can also calculate the magnetic induction, \mathbf{B} , from both $\mathbf{B} = \nabla \times \mathbf{A}$ and directly from Biot–Savart law. We define

$$T(t_1, t_2, t_3, t_4, t_5) = \frac{t_3}{t_4^2} \left[\frac{t_2 - t_5}{\sqrt{(t_2 - t_5)^2 + t_4^2}} - \frac{t_1 - t_5}{\sqrt{(t_1 - t_5)^2 + t_4^2}} \right]. \quad (B4)$$

It can be proved that the magnetic field created by the linear circuit is

$$B_x = \frac{\mu_0 I}{4\pi} \{T[a/2, -a/2, -z, \sqrt{(x-b/2)^2 + z^2}, y] + T[-a/2, a/2, -z, \sqrt{(x+b/2)^2 + z^2}, y]\}, \quad (B5)$$

$$B_y = \frac{\mu_0 I}{4\pi} \{T[-b/2, b/2, z, \sqrt{(y-a/2)^2 + z^2}, x] + T[b/2, -b/2, z, \sqrt{(y+a/2)^2 + z^2}, x]\}, \quad (B6)$$

$$B_z = \frac{\mu_0 I}{4\pi} \{T[a/2, -a/2, (x-b/2), \sqrt{(x-b/2)^2 + z^2}, y] + T[-a/2, a/2, (x+b/2), \sqrt{(x+b/2)^2 + z^2}, y] + T[-b/2, b/2, -(y-a/2), \sqrt{(y-a/2)^2 + z^2}, x] + T[b/2, -b/2, -(y+a/2), \sqrt{(y+a/2)^2 + z^2}, x]\}. \quad (B7)$$

¹L. D. Landau, E. M. Lifshitz, and L. P. Pitaevskii, *Electrodynamics of Continuous Media*, 2nd ed. (Pergamon, New York, 1984).
²D.-X. Chen, J. A. Brug, and R. B. Goldfarb, *IEEE Trans. Magn.* **27**, 3601 (1991).
³P. Rhodes and G. Rowlands, *Proc. Leeds Philos. Lit. Soc., Sci. Sect.* **6**, 191 (1954).
⁴R. I. Joseph, *J. Appl. Phys.* **38**, 2405 (1967).
⁵T. L. Templeton and A. S. Arrott, *IEEE Trans. Magn.* **23**, 2650 (1987).
⁶D.-X. Chen, C. Prados, E. Pardo, A. Sanchez, and A. Hernando, *J. Appl. Phys.* **91**, 5254 (2002).
⁷E. Pardo, A. Sanchez, and D.-X. Chen, *J. Appl. Phys.* **91**, 5260 (2002).
⁸L. Prigozhin, *J. Comput. Phys.* **144**, 180 (1998).
⁹C. P. Bean, *Phys. Rev. Lett.* **8**, 250 (1962).
¹⁰A. Sanchez and C. Navau, *Phys. Rev. B* **64**, 214506 (2001).
¹¹E. H. Brandt, *Phys. Rev. B* **58**, 6506 (1998).
¹²E. H. Brandt, *Phys. Rev. B* **54**, 4246 (1996).
¹³Th. Schuster, H. Kuhn, E. H. Brandt, M. V. Indenbom, M. Kläser, G. Müller-Vogt, H.-U. Habermeier, H. Kronmüller, and A. Forkl, *Phys. Rev. B* **52**, 10375 (1995).
¹⁴F. M. Araujo-Moreira, C. Navau, and A. Sanchez, *Phys. Rev. B* **61**, 634 (2000).
¹⁵C. Navau and A. Sanchez, *Phys. Rev. B* **64**, 214507 (2001).
¹⁶A. Badia and H. C. Freyhardt, *J. Appl. Phys.* **83**, 2681 (1998).
¹⁷A. Forkl and H. Kronmüller, *Phys. Rev. B* **52**, 16130 (1995).
¹⁸F. M. Araujo-Moreira, O. Florencio, C. Navau, E. Pardo, and A. Sanchez, *Physica C* **341–348**, 2055 (2000).
¹⁹J. R. Clem and A. Sanchez, *Phys. Rev. B* **50**, 9355 (1994).
²⁰E. H. Brandt, M. Indenbom, and A. Forkl, *Europhys. Lett.* **22**, 735 (1993).
²¹J. D. Jackson, *Classical Electrodynamics*, 3rd ed. (Wiley, New York, 1999), p. 215.